Biophysical Journal Volume 65 December 1993 2396–2407

Imaging in Five Dimensions: Time-Dependent Membrane Potentials in Individual Mitochondria

Leslie M. Loew,* Richard A. Tuft,‡ Walter Carrington,‡ and Fredric S. Fay‡

*Department of Physiology, University of Connecticut Health Center, Farmington, Connecticut 06030 and ‡Biomedical Imaging Group, Department of Physiology, University of Massachusetts Medical School, Worcester, Massachusetts 01655 USA

ABSTRACT Because of its importance in the chemiosmotic theory, mitochondrial membrane potential has been the object of many investigations. Significantly, however, quantitative data on how energy transduction might be regulated or perturbed by the physiological state of the cell has only been gathered via indirect studies on isolated mitochondrial suspensions; quantitative studies on individual mitochondria in situ have not been possible because of their small size, their intrinsic motility, and the absence of appropriate analytical reagents. In this article, we combine techniques for rapid, high resolution, quantitative three-dimensional imaging microscopy and mathematical modeling to determine accurate distributions of a potentiometric fluorescent probe between the cytosol and individual mitochondria inside a living cell. Analysis of this distribution via the Nernst equation permits assignment of potentials to each of the imaged mitochondrial membranes. The mitochondrial membrane potentials are distributed over a narrow range centered at −150 mV within the neurites of differentiated neuroblastoma cells. We find that the membrane potential of a single mitochondrion is generally remarkably stable over times of 40–80 s, but significant fluctuations can occasionally be seen. The motility of individual mitochondria is not directly correlated to membrane potential, but mitochondria do become immobile after prolonged treatment with respiratory inhibitors or uncouplers. Thus, three spatial dimensions, a key physiological parameter, and their changes over time are all quantitated for objects at the resolution limit of light microscopy. The methods described may be readily extended to permit investigations of how mitochondrial function is integrated with other processes in the intact cell.

INTRODUCTION

The energy released during the oxidation reactions in the mitochondrial respiratory chain is stored as an electrochemical potential consisting of a transmembrane electrical potential (V_{mit}) of about −180 mV and a proton gradient of about 1 pH unit; this energy is then able to drive the synthesis of the ATP required to fuel the cell's energy-dependent processes (Mitchell, 1961; Chance et al., 1977; Nicholls, 1982; Ferguson, 1985). This key system in cell biology has been the subject of thousands of biochemical and biophysical investigations. Therefore, most of the details have been elucidated, and the validity of the energy transduction mechanism is broadly accepted; some areas of controversy remain, however (Tedeschi, 1980; Ferguson, 1985). In addition, it has not been possible to quantitatively follow V_{mit} inside living cells. This has impeded progress toward understanding how the process of energy transduction is controlled and regulated in situ.

Previous studies of V_{mit} can generally be divided into two categories—quantitative studies on isolated mitochondrial suspensions and qualitative studies on mitochondria within intact living cells. The former used either radioactive or fluorescent lipophilic cations for which distribution between the mitochondrial and bathing media could be readily determined. After appropriate calibration by changing the ionic gradient in the presence of ionophore and correcting for background probe binding, the average V_{mit} of the population is obtained (Smith, 1988). Interestingly, experiments on isolated single cuprozine-treated giant mitochondria have been possible with microelectrodes (Tedeschi, 1980) and have produced results sharply disparate to the more common approaches. The work of Lan Bo Chen and his colleagues best exemplifies the approaches used with intact cells. They developed a protocol for staining cells with a cationic dye, rhodamine 123, such that the brightness of the mitochondria under a fluorescence microscope qualitatively indicates their V_{mit} (Johnson et al., 1981; Chen, 1988). More recently, a new dye that changes its emission wavelength as a function of V_{mit} was introduced by the Chen group; while the emission shift can be used to quantitate average membrane potential in mitochondrial suspensions (Smiley et al., 1991), it can only provide qualitative indications of V_{mit} in cells (Reers et al., 1991).

An approach toward a more quantitative assessment of V_{mit} within intact cells was based on the development of the reversible cationic redistribution dyes tetramethylrhodamine ethyl and methyl esters (TMRE and TMRM, respectively; Ehrenberg et al., 1988). These dyes, members of the rhodamine family, are rapidly and reversibly equilibrated across membranes in a voltage-dependent manner governed by the Nernst equation. It was possible to distinguish between changes in mitochondrial and plasma membrane potential with video microscopy (Farkas et al., 1989), but the mitochondria are too small to permit accurate intensity measurements with a widefield microscope. The difficulty is that both the fluorescence from the mitochondrion and an adjacent equivalent cytosolic volume have to be determined without

Received for publication 10 June 1993 and in final form 23 August 1993.

Address reprint requests to Dr. Leslie M. Loew, Department of Physiology, School of Medicine, University of Connecticut Health Center, 263 Farmington Avenue, Farmington, CT 06030-3505.

0006-3495/93/12/2396/12 $2.00

contributions from fluorescence emanating from regions above or below. This problem cannot be solved by simply using a thin flat cellular region, such as the lamelipodium of a fibroblast, even if individual mitochondria can be resolved, because the thickness of the volume sampled by the widefield microscope dilutes the intensity of a mitochondrion relative to a cytosolic or extracellular region. Confocal microscopy limits the thickness of the volume from which fluorescence is detected, and this technique has been used to provide better estimates of the required intensities (Farkas et al., 1989; Loew, 1993). But V_{mit} obtained in this way can only be considered a lower limit because even a confocal optical section may be significantly thicker than a given mitochondrion and is not necessarily accurately centered on it. Current generation confocal microscopes also have the disadvantages of being slow and requiring high intensity laser excitation; these features, respectively, preclude accurate measurements of motile mitochondria and prevent accumulation of three-dimensional (3D) datasets or time series without significant photobleaching and phototoxicity.

A stratagem complementary to confocal microscopy for eliminating out-of-focus contributions in a microscope image involves computer algorithms that use the experimental 3D optical characteristics of the microscope to deconvolve 3D widefield datasets (Agard, 1984; Carrington and Fogarty, 1987; Agard et al., 1989; Fay et al., 1989). This method effectively takes the out-of-focus fluorescence measured in the experimental data and restores it to its appropriate point of origin. Image restoration has been confined to studies where precise high resolution 3D structural information is required (the primary application of confocal microscopy, as well). In this paper, we show that it can also be used to obtain accurate fluorescent intensities from objects at or even below the resolution limit of the light microscope. By employing a cellular preparation with a uniform population of mitochondria, a permeable cationic dye which distributes according to the Nernst equation, a fast 3D microscope to freeze mitochondrial motion, and mathematical modeling to calibrate intensities in restored 3D images, V_{mit} may be determined from individual mitochondria inside living cells.

MATERIALS AND METHODS

N1E-115 neuroblastoma cells were induced to differentiate after plating on no. 1 coverslips according to published procedures (Kimhi et al., 1979). A coverslip was mounted on a microscope chamber (Loew, 1993) thermostatted to 37°C and equilibrated with 100 nM TMRE (Ehrenberg et al., 1988) in a balanced salt solution containing 10 mM glucose, 120 mM NaCl, 4 mM KCl, 1 mM KH_2PO_4, 1 mM $MgSO_4$, 1.3 mM $CaCl_2$, a 1:50 dilution of minimal essential medium amino acids (Sigma Chemical, Co., St. Louis, MO) and 10 mM HEPES buffer adjusted to pH 7.4. The microscope chamber was connected to a manifold that permitted exchange of solutions as for the introduction of agents to perturb V_{mit}. All solutions for exchange contained the same concentration of TMRE (100 nM) as the original equilibration buffer.

A rotatable stage on a custom-built epifluorescence microscope permitted the alignment of a neurite with the long dimension of the exposed 73 × 512 pixels on a square 512 × 512 charge-coupled device (ccd) chip in a cooled frame transfer ccd camera. Charge may be rapidly transferred to the masked portion of the chip so that seven images can be acquired in rapid succession before the chip has to be read out. A piezoelectric driver connected to a Nikon 60× N.A.1.4 objective is programmed to change the focus along the optical (z) axis in concert with these seven successive exposures of the ccd. The exposure time for each objective position was set typically to 5 ms; a time interval between focus changes was set at 20 ms to permit settling of coverslip drumming vibrations resulting from mechanical coupling to the oil immersion objective. Sufficient excitation intensity to permit such short exposures is provided by the 514 nm line of an argon ion laser running typically at 250 mW. A dichroic mirror-emission filter combination optimized for rhodamine fluorescence (Omega Optical, Inc., Brattleboro, VT) comprised the remaining optics. A diagram of the apparatus, including timing of the excitation and camera shutters and the objective movement, is given in Fig. 1. Full details of this apparatus will be provided elsewhere.

The 3D dataset thus obtained was processed by the image restoration algorithm described by Carrington et al. (Carrington, 1990; Carrington et al., 1990). First, the microscope optical characteristics are measured by obtaining an experimental point spread function (PSF). The PSF is determined by acquiring a 3D image of a subresolution fluorescent bead consisting of at least 20 xy planes at 0.3-μm z spacing. Beads with rhodamine excitation and emission characteristics and a narrow size distribution centered at 185 nm are commercially available (Molecular Probes, Inc., Eugene, OR) and adhere to the coverslip containing the neuronal cells. A PSF was determined for every coverslip to ensure that the optics were accurately defined for each experiment. Before restoration, the data are digitally corrected for background intensity and small heterogeneities in the ccd sensitivity. The response of a camera pixel, g_i, to a 3D dye density, $f(x, y, z)$, is then

$$g_i = \int\int\int k_i(x, y, z) f(x, y, z)\, dx\, dy\, dz \qquad (1)$$

where $k_i(x, y, z)$ is the PSF shifted to the position on which the camera pixel is focused. The restoration procedure is then to choose the non-negative $f(x, y, z)$ that minimizes

$$\Sigma \left| g_i - \int\int\int k_i(x, y, z) f(x, y, z)\, dx\, dy\, dz \right|^2 + \alpha \int\int\int |f(x, y, z)|^2\, dx\, dy\, dz \qquad (2)$$

The iterative numerical algorithm that performs this minimization has been described (Carrington, 1990). The formulation of the imaging process in Eq. 1 as discrete data and continuum dye density allows us to calculate the restored dye density on a different pixel grid than the sampling grid of the measured image. We use that flexibility here to space the optical sections at z = −1.2, −0.6, −0.3, 0, +0.3, +0.6, and +1.2 μm. This ability to skip planes of data allows us to span the whole cell from top to bottom with seven planes and still obtain high axial resolution. The output of the restoration is a dataset that includes 9 xy planes at equal 0.3-μm z spacings. Restoration of a single 3D image typically requires 45 min on a Silicon Graphics Inc. (Mountain View, CA) VGX computer with four 33 MHz RISC R3000 microprocessors.

Image analysis was performed on Silicon Graphics Inc. workstations using a suite of custom imaging software written by Kevin Fogarty and Doug Bowman. A key component of this analysis was an interactive 3D segmentation procedure that permitted determination of the volume, x, y, z coordinates of the centroid, and the intensity of individual mitochondria. These data were transferred to a spreadsheet program (Quattro Pro, Borland International, Inc., Scotts, Valley, CA) on a personal computer for calculation of V_{mit} and mitochondrial motilities.

RESULTS

Fast 3D imaging of TMRE fluorescence in neurites

The neurites of N1E-115 neuroblastoma cells proved to be excellent subjects for this investigation. The long narrow

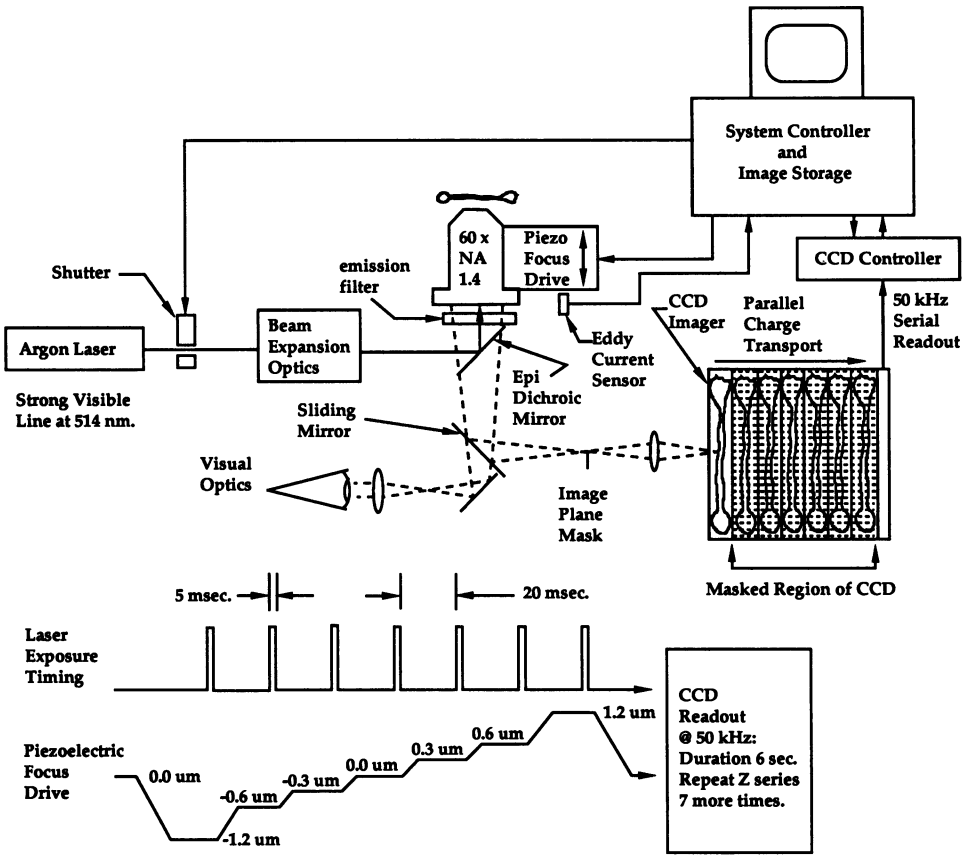

FIGURE 1 System and timing diagram of the fast 3D microscope. An argon laser (model 2025; Spectra Physics, Mountain View, CA) provides 250 mW of $\lambda = 514$ nm radiation. Exposures are timed by a fast shutter (Uniblitz, Rochester, NY; LS2 shutter and D122 driver). The laser beam is expanded and directed to the epi-illumination optics of a custom built inverted microscope, providing a widefield illumination flux of $\sim 1 \times 10^{21}$ photons cm $^{-2}$ s^{-1} at the specimen plane of the microscope. The fluorescent emission passes through a 550-nm longpass filter (Omega, Brattleboro, VT) and an intermediate image is formed by a plan apo 60× N.A.1.4 objective (Nikon, Garden City, NY). A mask placed in the plane of the intermediate image limits the field that is reimaged onto a 512 × 512 pixel ccd camera (Photometrics, Tucson, AZ, model CC200 controller and CH250 camera head with Tektronix TK512 CCD). The imaged specimen field is ~10 × 67 μm (73 × 512 pixels, 130 nm/pixel). The masked area on the ccd is used to store up to 6 earlier images, which are shifted under the mask by parallel charge transport between exposures. At the same time, the focus is changed by a piezoelectric translator (model P-244.27 PZT and P-267 controller; Polytec Optronics, Costa Mesa, CA) attached to the center of mass of a counterweighted objective carrier. This drive configuration can attain stepped objective translations at rates of 1 μm/ms, but ~20 ms must be allowed for relaxation of the deformations introduced in the chamber coverslip by coupling of the objective motion through the immersion oil. Typical exposure times and focus positions are as illustrated. After the ccd is filled with a 7-image through-focus series, the ccd is read out (~6 s) and the process repeated to obtain a time series.

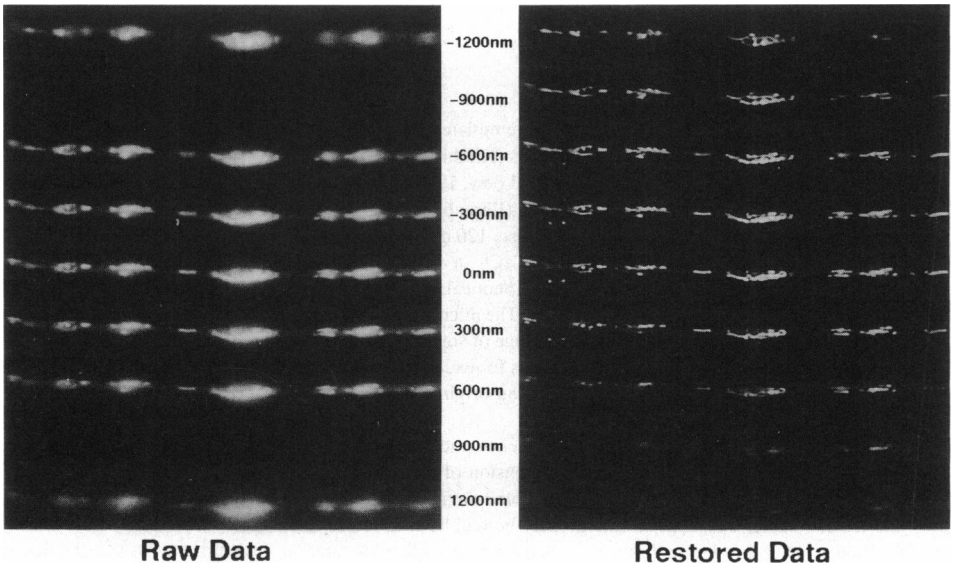

FIGURE 2 Rapid acquisition and image restoration of fluorescence from a neurite equilibrated with 100 nM TMRE. The left side of the figure shows a series of images obtained at the indicated set of z positions. The series on the right shows the result of processing the data with the restoration algorithm; enhanced resolution and contrast are evident.

cylindrical neurites, with diameters of typically 2 μm, were an ideal geometry to be imaged onto the 73 × 512 pixel exposed area of a cooled ccd camera which had the other 6/7 of its area masked. The camera is part of a custom-built 3D widefield microscope (Fig. 1), which features piezoelectric driven focus, high laser intensity excitation (for short exposure times), and frame transfer ccd technology (for rapid image acquisition). A through focus series of images, as shown on the left of Fig. 2, can be obtained in this way in only 155 ms. Of all the mitochondria analyzed (vide infra), 95% travel less than 1 pixel during the 155 ms required for data collection; the motion of mitochondria never reaches more than 3 μm/s, so that the maximum movement during the acquisition of the full 3D image is no more than 3 pixels. The focus is stepped through a series of increments, as indicated in Fig. 2, designed to bracket the fluorescence emanating from the neurite volume while maintaining high resolution along the *z*-axis in the center of the 3D dataset.

The right side of Fig. 2 shows the 3D dataset resulting from the application of the restoration algorithm to the experimental data. The relative contrast between mitochondrial and cytosolic fluorescence increases from 14:1, in the raw images, to 100:1 in the restored images. Analysis of electron micrographs (Fig. 3) reveals that the mitochondria are generally cylindrical objects oriented parallel to the long axis of the neurite with variable lengths and rather uniform diameters of 230 ± 18 nm. After restoration, the typical cross section of fluorescence perpendicular to its long axis (the *x*-axis in Fig. 2) of a mitochondrion is such that 95% of the fluorescence is contained within a volume which has a *y* dimension of 0.3 μm and a *z* dimension of 1.1 μm. The restoration is, therefore, not perfect, but all the mitochondrial fluorescence has been constrained to within the imaged volume. In order to compensate for the small amount of residual blurring within this volume and permit us to determine accurate membrane potentials, a modeling procedure was implemented and is detailed in the following section.

Determination of V_{mit} for individual mitochondria

Ideally, to determine V_{mit}, the Nernst equation is applied to the ratio of fluorescence from an interior point within the mitochondrion and an equally small volume within the cytosol. A condition that must be met, however, is that the accumulation of dye must be driven only by electrical potential differences and not by any nonspecific binding. TMRE has appropriate properties to generally ensure low nonspecific binding and, further, any such contribution can be determined and accounted for in the membrane potential calculation (Farkas et al., 1989; Loew, 1993). In the case of N1E-115 cell neurites, we find that nonpotentiometric binding is so low that it cannot be detected. This was established by depolarizing the cell and mitochondrial membranes via treatment with a high $[K^+]$ medium containing the potassium-selective ionophore valinomycin (Fig. 4). Any residual mitochondrial fluorescence is attributed to passive binding of the dye to mitochondrial membranes. Following such treatment, the contrast between mitochondria and cytosol is essentially abolished indicating no significant passive binding of TMRE to mitochondrial components. The experiment of Fig. 4 was repeated with TMRE concentrations up to 5 μM—50 times the standard concentration—with no significant fluorescence from structures that could be identified as mitochondria; a diffuse cytosolic fluorescence no more than 1.15 times that of background could be detected under these extreme conditions. We have also established that, in untreated cells, a linear relation exists between mitochondrial

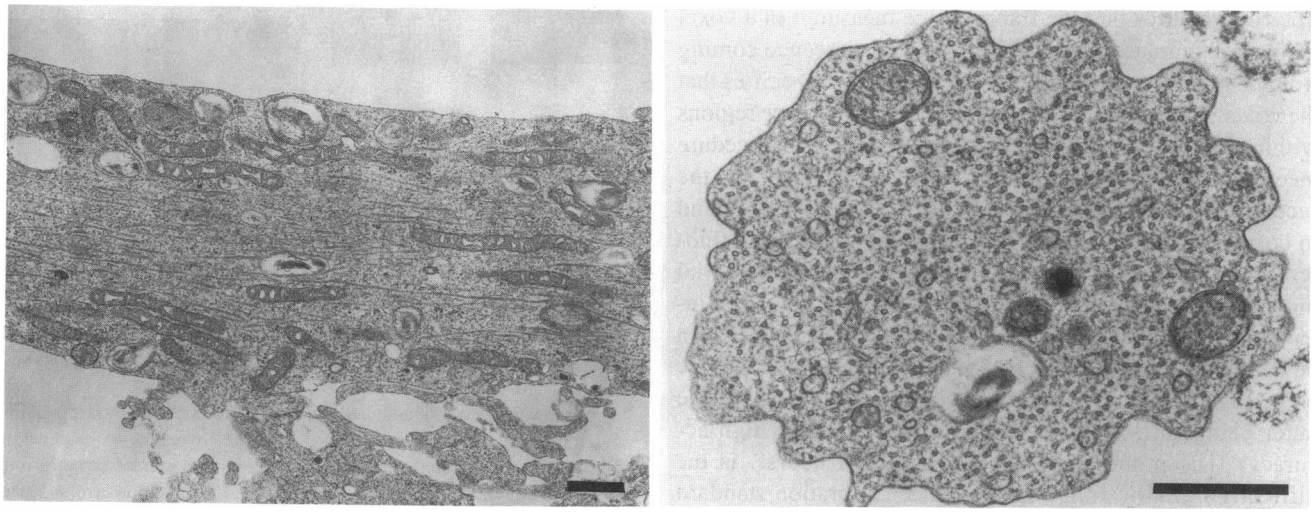

FIGURE 3 Thin section transmission electron micrographs of neuroblastoma cell neurites. The left shows a neurite sectioned in a plane containing the long axis (i.e., parallel to the substrate). Mitochondria with variable lengths but remarkably uniform widths are arrayed alongside microtubules, which appear to fill the neurite volume. The image on the right shows a section perpendicular to the long axis of a neurite revealing round mitochondrial cross sections. Note the profusion of microtubules revealed as small circular structures in this orientation of the neurite. The scale bar in each image corresponds to 500 nm.

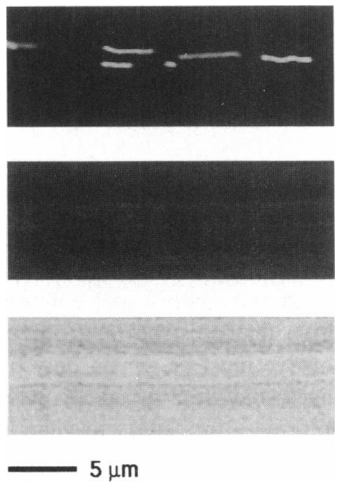

FIGURE 4 Depolarization of a neurite equilibrated with 100 nM TMRE results in complete loss of mitochondrial fluorescence. The top image is a central plane of the 9 optical sections of a restored 3D dataset. The contrast between the mitochondrial and cytosolic fluorescence intensities is typically a factor of 200. The middle image shows the same cell following treatment with 1 μM valinomycin in a medium in which Na^+ has been replaced with K^+ and with the intensity scale preserved; this depolarizing medium still contains 100 nM TMRE. The bottom image is the depolarized cell with the scale stretched to reveal any residual fluorescence (the speckled pattern is underlying noise which is not visible in the normal scale).

fluorescence and [TMRE] up to ~400 nM in the extracellular bathing medium, at which point self-quenching of the highly concentrated intramitochondrial dye becomes appreciable (Ehrenberg et al., 1988). Therefore, if the ratio of fluorescence emanating from a 3D picture element (voxel) situated within a mitochondrion to that emanating from a cytosolic voxel could be determined, it should accurately reflect the ratio of the respective dye concentrations.

Two additional conditions, however, must be met to assure that mitochondrial fluorescence is accurately determined. The first requires that the fluorescence measured in a voxel not be contaminated with out-of-focus fluorescence coming from neighboring mitochondria and the second specifies that the voxel intensity not be diluted by low fluorescence regions within the broad depth of field. The restoration procedure meets the first condition, but only comes close to meeting the second. To estimate the extent to which this is a problem and to correct for it, one could image and then restore the fluorescence from a standard cylinder with typical mitochondrial dimensions and with a known concentration of dye. The intensity from a central pixel in this restored object could then be compared to the intensity from a pixel centered in a large object also containing a known concentration of dye (the latter being sufficiently large to be restored with high accuracy). The problem with this scheme, of course, is the difficulty in fabricating a fluorescence calibration standard with the dimensions of a 230-nm diameter cylinder. We adopted an alternative approach in which the unprocessed 3D microscope image of such an object is simulated by blurring a computer model of a mitochondrion. The model is a cylinder with a length of 1 μm and a diameter of 230 nm containing pixels all set at 10^4 intensity units. This model is blurred using the PSF taken directly from the experimental coverslip. The model and the PSF are created with pixel sizes in each dimension which are ⅓ normal size to avoid pixelization artifacts during the blurring process. The blurred model is then reduced to the normal resolution, inserted into a real neurite by image addition to include a realistic noise level, and, finally, restored with the same PSF used to restore all the experimental images. The procedure is illustrated in Fig. 5. Typically, a central pixel needs to be corrected for incomplete restoration by between a factor of 3 and 4. (As detailed below, the logarithmic form of the Nernst equation translates this into a correction of between 29 and 36 mV out of a total average V_{mit} of −150 mV.)

Based on these considerations, a modified form of the Nernst equation employing the measured fluorescence in individual mitochondria in restored images is used to calculate V_{mit}:

$$V_{mit} = -60 \text{ mV} \log\left[\frac{\text{cal} \cdot F_{mito}}{F_{cyt}}\right] \quad (3)$$

where F_{mito} is the intramitochondrial fluorescence; F_{cyt} is the cytosolic fluorescence; and cal is the calibration factor obtained from the mitochondrial model. In order to accommodate any experiment to experiment changes in the optical characteristics of the microscope, point spread functions are determined from fluorescent microspheres added to the same coverslip onto which the cells are plated. These PSFs are used for both the restoration and model-based calibrations for the data from the corresponding coverslip.

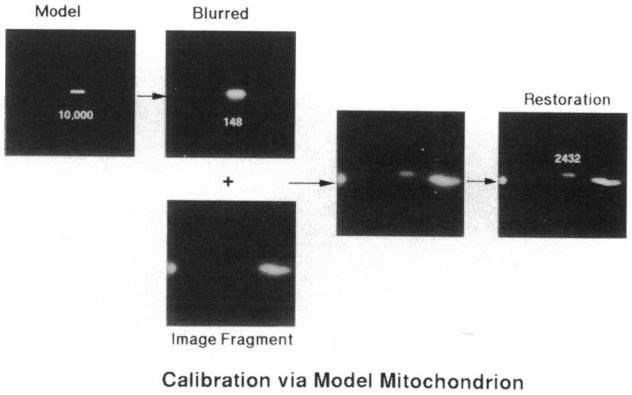

FIGURE 5 Model mitochondria are used to calibrate the accuracy of the restorations. A model cylindrical mitochondrion (*upper left*) is constructed with a length of 1000 nm and a diameter of 230 nm (from the electron microscopy data) and an assigned intensity of 10,000. The model is blurred with a point spread function obtained from the coverslip, which generated the data to be calibrated. The blurring operation is carried out at 3 times the pixel resolution of the microscope to avoid pixelization errors. The resultant blurred model is reduced to the appropriate pixel dimensions and combined with a 3D image fragment to introduce experimental noise. This image is then restored with the same point spread function used on the data. The maximum intensity of the restored model is compared to the original model to generate a calibration factor. The above images are all midplanes of 3D sets.

A restored image is segmented by a 3D thresholding technique which individually isolates each mitochondrion and determines key parameters, including the maximum, minimum, and mean intensities, the x, y, and z coordinates of the weighted center of gravity, and the mitochondrial volume. The maximum intensity, emanating from a pixel deep within the mitochondrial volume, is used as F_{mito} in Eq. 3. F_{cyt} is obtained by taking the average intensity within mitochondria-free regions in the center of the neurite. Mitochondria that are intertwined or closely overlapping are not included. The membrane potentials obtained from such an analysis on a single neurite are shown in the bottom of Fig. 6 *a*; a

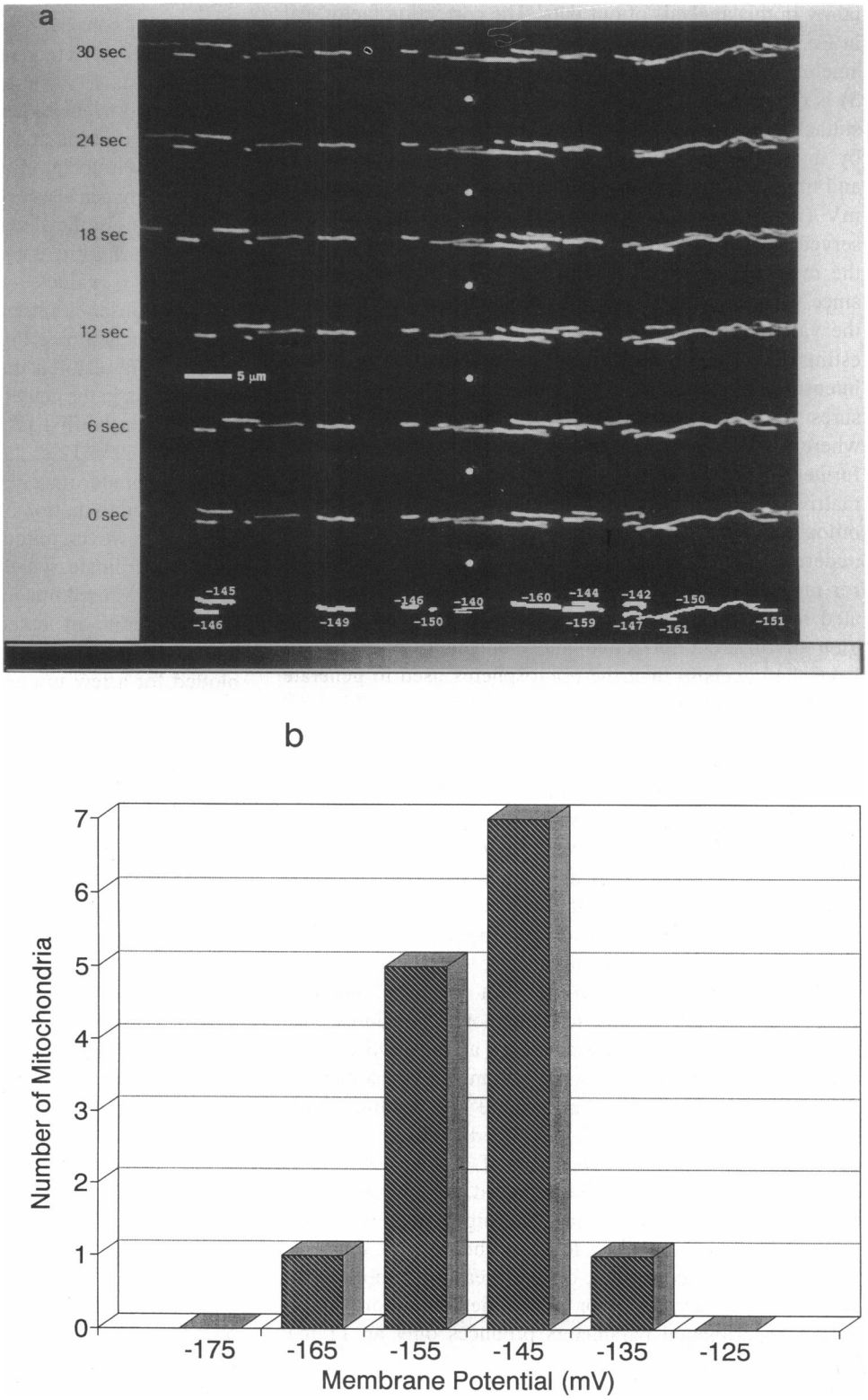

FIGURE 6 Assignment of membrane potentials to motile mitochondria. (*a*) An experiment in which individual mitochondria have been analyzed. The bottom image indicates the membrane potentials of each analyzed mitochondrion. A time sequence of projections of the 3D datasets onto a single plane is displayed above with times, in seconds, indicated. Saltatory motion of the mitochondria is evident. A fluorescent calibration bead is seen toward the center of each image; its intensity saturates the display, which was scaled to best visualize the mitochondria, but is within the range of the 16-bit image. (*b*) Histogram of membrane potentials in individual mitochondria from the initial time point of the neurite in *a*.

histogram of the V_{mit} distribution for this neurite is shown in Fig. 6 *b* and indicates a fairly narrow range of membrane potentials. The standard deviations from the mean V_{mit} within a neurite ranged between 4 and 12 mV; the average of these means was −150 mV (SD 11 mV) for 17 neurites on 8 separate coverslips containing 347 analyzed mitochondria.

It is important to consider sources of error and uncertainty in this analysis of our data. The correction factor, cal in Eq. 3, is based on modeling of a cylinder of 230-nm diameter. The distribution of mitochondrial diameters (Fig. 3) is characterized by a SD of ±18 nm, however. The resultant uncertainty in the correction factor was determined by modeling cylinders of 248 and 212 nm, as in Fig. 5, and translates, ultimately, into an uncertainty in V_{mit} of ±4 mV (i.e., a narrower predicted distribution than the observed range). Similarly, the actual volume occupied by the matrix is smaller than the full cylinder of our model since the thickness of the inner and outer membrane, and the variable space between them could not be accurately estimated for each mitochondrion. Choosing the maximum intensity voxel within each analyzed mitochondrion ensures that the volume being sampled is from a region where the matrix closely fills the cylindrical cross section; further, from the electron micrographs, we estimate the matrix volume to be always greater than 80% of the total mitochondrial volume and this translates into a possible underestimate of V_{mit} by no more than 6 mV. A small error may be introduced because the mitochondria are situated inside the cytosol and therefore surrounded by a region of different refractive index and a distance further from the coverslip than the microspheres used to generate the PSFs; for the thin neurites used in this study, this kind of error is insignificant. Finally, the valinomycin/K^+ depolarization experiments (Fig. 4) cannot completely rule out the possibility of significant background binding. Firstly, the mitochondria appear to swell and perhaps lyse under these conditions; secondly, we have not been able to obtain images of depolarized neurites at dye concentrations as high as would pertain in the matrix of a fully energized mitochondrion. Therefore, it is possible that we could be missing some background binding. If we assume that all the cytosolic contrast seen in the valinomycin/K^+ depolarization experiment is due to mitochondrial fluorescence and extrapolate this up to account for a 1000-fold concentration of dye in the matrix, a maximum overestimate of 20 mV due to neglect of background dye binding is derived. To summarize, identifiable uncertainties in the measurements can affect the precision of V_{mit} by ± 4 mV; with respect to accuracy, the reported values may be up to 6 mV too low or 20 mV too high. In general, the method is quite insensitive to errors because of the logarithmic dependence of V_{mit} on the measured fluorescence (Eq. 3)—even a 50% error in the determination of one of the experimental parameters produces only an 11 mV error in V_{mit}.

Time dependence of V_{mit}

Fig. 6 also shows a time series of 8 images collected at intervals of 6 s. Each image is a projection of the highest intensity pixel along the *z*-axis of a 3D image onto a single *xy* plane. The membrane potential distribution shown in the binary image at the bottom of the figure corresponds to the analysis of the first time point. Saltatory motion of some of the mitochondria over this time course is evident with speeds (0–3 μm/s) consistent with those found in video-enhanced differential interference contrast studies of axonal transport (Martz et al., 1984; Forman et al., 1987). This experiment was devised to probe for a correlation between the motility of a mitochondrion and its membrane potential. Analysis of hundreds of mitochondrial potentials gave no significant correlation between these properties.

Interestingly, however, an unexpected phenomenon was detected during the course of these studies. While most individual V_{mit} values remain constant over the 42-s time course of observation, occasional mitochondria display significant fluctuations. Fig. 7 *a* displays 2D projections of a series of 3D restored images taken 6 s apart. The long mitochondrion in the center of the image, labeled 4, has a stable intensity for the first 12 s but becomes significantly dimmer during the next 12 s; the intensity recovers thereafter. Had this data come from a 2D confocal image, such results might be attributed to motion of the mitochondrion out of the plane of focus; however, mitochondrion 4 remains at an essentially fixed *z* coordinate, which is well within the sampled volume of the 3D restored image. The change in intensity, therefore, is most readily attributed to a change in intramitochondrial dye concentration. The intensities are translated into V_{mit} and plotted for a few mitochondria in Fig. 7 *b*. Other than mitochondrion 4, mitochondria in the image have relatively stable intensities at each of the 6 time points. Parenthetically, this attests to the reproducibility and consistency of the method as well as to the photostability of the dye. Potentials from individual mitochondria could be monitored for 8–12 time points, corresponding to 56–84 exposures to the laser excitation source, after which photodynamic damage became evident (plasma membrane blebbing and mitochondrial swelling). In aggregate, large fluctuations in the range of 20 mV and lasting up to 24 s were found in 10 of the 307 mitochondria, which were monitored 8 times each over a 42-s time interval. These 10 events took place in 7 different neurites and appeared generally to correspond to depolarizations, although the limited number of time points made it difficult to distinguish the baseline potential from the fluctuation in some of the cases.

Response of V_{mit} to uncouplers and respiration inhibitors

Treatment of the cells with 1 μM FCCP, a potent protonophore uncoupler, effects complete release of TMRE from the mitochondria in less than 10 s (Fig. 8). Since readout of the ccd chip requires 6 s, the kinetics of this process could not

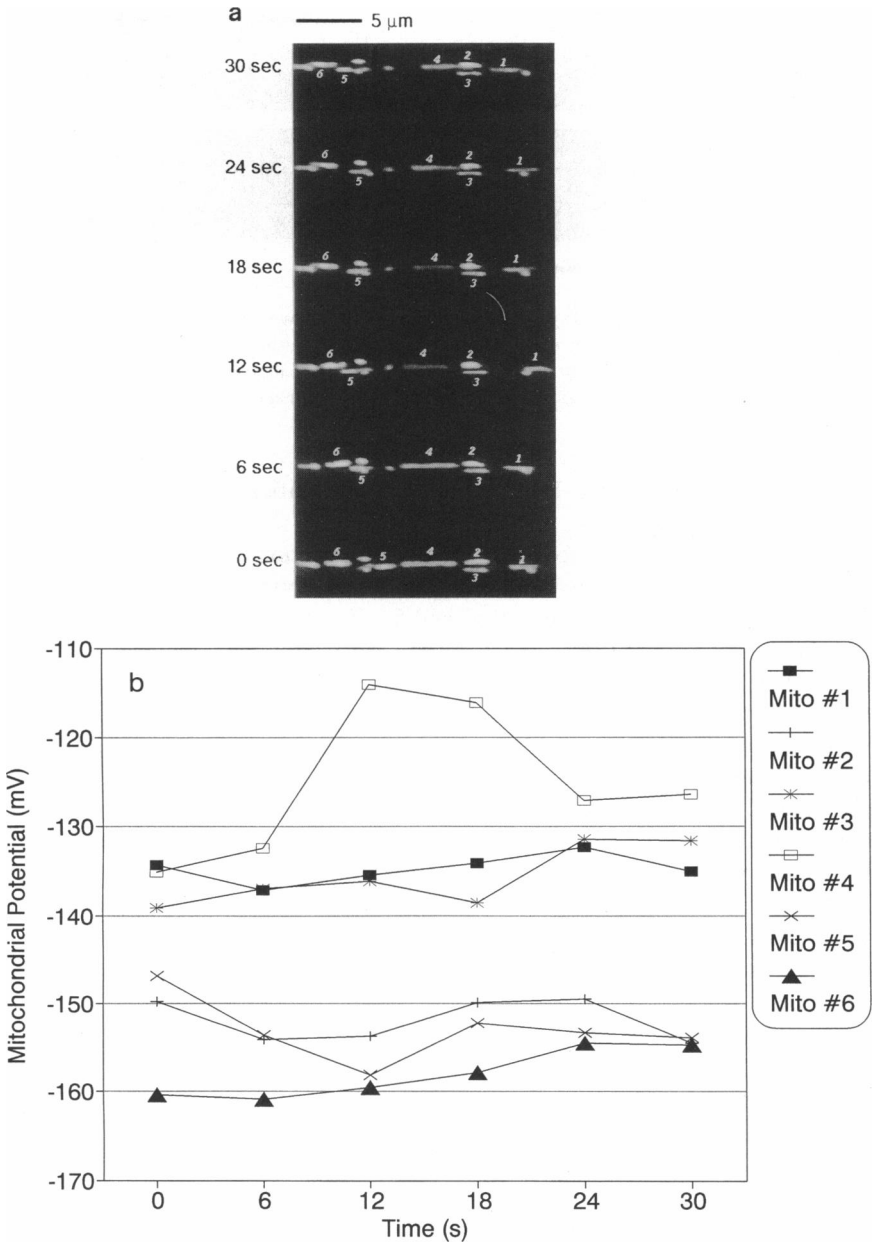

FIGURE 7 Mitochondria occasionally display large membrane potential fluctuations. (*a*) Time series of restored images taken at 6-s intervals. Notice the loss of intensity in mitochondrion 4 in the 3rd and 4th time points. (*b*) V_{mit} is plotted for each of the labeled mitochondria, indicating the magnitude of the fluctuation in mitochondrion 4.

be followed, but it attests to the ability of the dye to resolve fast depolarization of the mitochondria in these cells. Interestingly, treatment of the cells with 0.1 μM FCCP depolarizes the mitochondria more slowly and incompletely. This behavior is illustrated in Fig. 9 for a series of neurites on the same coverslip. Before treatment with the uncoupler, a histogram of V_{mit} from a single neurite shows the typical average baseline of ~−150 mV (Fig. 9 *a*). Fig. 9 *b* shows histograms of a neurite immediately before and 2 min after introduction of 0.1 μM FCCP. The uncoupler produces a small depolarization in each mitochondrion with an average V_{mit} of −157 mV before the drug and −150 mV after 2 min of FCCP exposure; because the potential of individual mitochondria are, generally, extraordinarily stable, (as discussed in connection with Fig. 7), this small depolarization is significant. Unfortunately, we found that in the presence of uncouplers or mitochondrial inhibitors, the mitochondria become extremely sensitive to photodynamic damage. After drug treatment, fluorescence is lost from mitochondria after two or three 3D images have been acquired; an adjacent region of the same neurite is unaffected. Therefore, after treatment with FCCP, we could not monitor the time course of V_{mit} changes for a fixed set of mitochondria. A third neurite observed 5 min after the introduction of FCCP gives an average V_{mit} of −135 mV (Fig. 9 *c*); a fourth neurite (Fig. 9 *d*) observed after 28 min had an average V_{mit} of −128 mV. While it would have been preferable to follow a single set of mitochondria, these results clearly indicate that 0.1 μM FCCP induces a moderate depolarization of 20–30 mV. The mitochondria are, thus, able to continue pumping enough

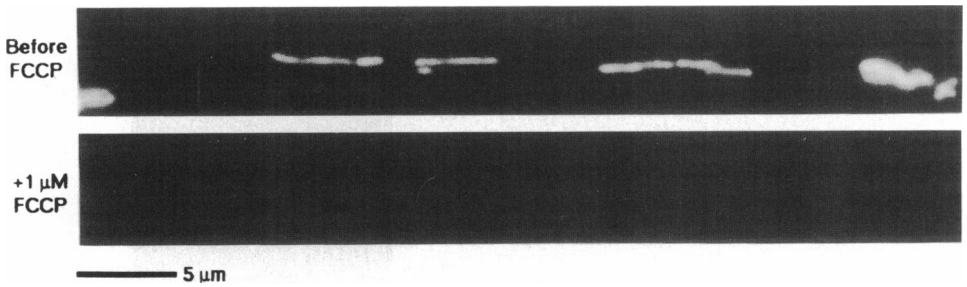

FIGURE 8 Mitochondria quickly lose TMRE fluorescence following treatment with 1 μM FCCP. The top image shows a neurite before treatment with the uncoupler, and the bottom shows the same neurite 10 s after flushing the chamber with an identical 100 nM TMRE buffer to which the uncoupler had been added. This was the minimum time required to assure temperature equilibration and permit refocusing of the neurite in brightfield illumination. The data were collected as single planes focused on the center of the neurite and were, therefore, not restored.

protons against this added load to maintain a significant membrane potential.

This depolarization has no direct effect on the motion of the mitochondria; comparison of histograms of individual mitochondrial speed before (Fig. 9 *a*) and 5 min after (Fig. 9 *c*) treatment with 0.1 μM FCCP reveals no qualitative differences in the dynamics of these organelles. In addition, as in the case of untreated cells, there is no correlation between the motility of individual mitochondria and their V_{mit}. Given enough time, however, all motion stops. Fig. 9 *d* shows that after 28 min of exposure to 0.1 μM FCCP, V_{mit} in a neurite on the same coverslip remains at −128 ± 6 mV, but the mitochondria have stopped all their saltatory motion.

Similar results are obtained with the drug antimycin A, an inhibitor of mitochondrial electron transport (Singer, 1979). A single neurite was monitored before and after treatment with 1 μM antimycin A. The initial average V_{mit} was 149 ± 8 mV; 2 min posttreatment, the average V_{mit} fell to −108 ± 8 mV. The mitochondrial motion was not affected at this 2-min time point. A different neurite on the same coverslip was imaged after 5 min of exposure to the drug; the membrane potential remained stable (−112 ± 8 mV), but the motion had ceased.

DISCUSSION

This study permits us for the first time to assess the respiratory activity of individual mitochondria inside a living cell. The mitochondria within a neurite have a relatively uniform membrane potential with standard deviations ranging from 4 to 12 mV for 17 different cells containing a total of 347 analyzed mitochondria; the unweighted mean of the average

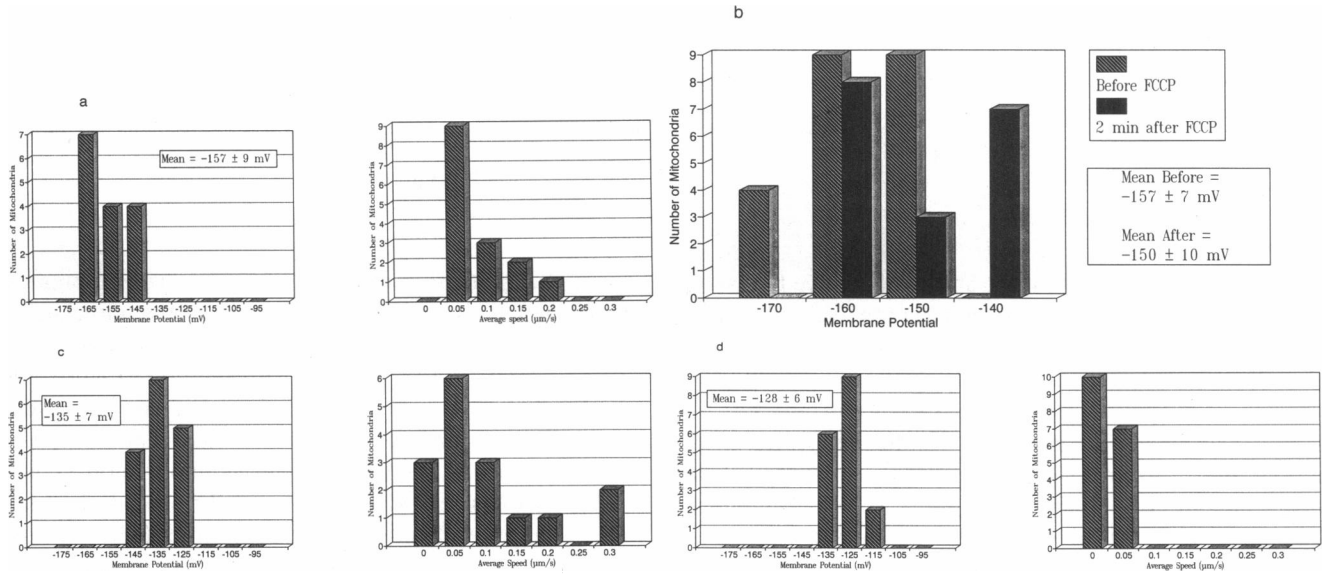

FIGURE 9 Mitochondrial potential is depolarized to a new level by an uncoupler. Cells were mounted on the thermostatted chamber and imaged before and after introduction of medium containing 0.1 μM FCCP. After restoration, V_{mit} was calculated according to Eq. 3; in addition, the cartesian coordinates of the centroids of each mitochondrion in a 42-s time series of 8 3D images was used to calculate the average speed of the individual mitochondria. All data were obtained from neurites on a single coverslip, but, because phototoxic effects became evident after too much light exposure, several neurites had to be sampled. (*a*) Histograms of V_{mit} and speed distributions from a neurite before FCCP treatment. (*b*) Histograms of V_{mit} from the same neurite before and 2 min after treatment with 0.1 μM FCCP. (*c*) Potential and motion histograms in a third neurite 5 min after 0.1 μM FCCP. (*d*) A fourth neurite, 28 min later, displays a stable potential but a loss of saltatory motion.

V_{mit} between these 17 neurites is -150 ± 11 mV. This distribution is wider than what might be predicted based on analysis of possible errors affecting the precision of the measurements. We feel that the width of the distribution is probably real, therefore, and reflects a range of respiratory activity among mitochondria. Such information could not, of course, be derived from bulk measurements on mitochondrial suspensions. An attempt to assess factors that could affect the accuracy of the measurements focused on uncertainties in the level of nonpotentiometric dye binding and a possible overestimate of the matrix volume. Based on these possible errors, the values of V_{mit} reported in this study could be up to 20 mV too high or 6 mV too low.

That the mitochondria are in state 3 respiration is suggested (Scalettar et al., 1991) by the "condensed" morphology shown in the electron micrographs (Fig. 3) of the characteristically cylindrical mitochondria in the neurites. Electron micrographs of mitochondria in the soma of these cells (data not shown) indicate that these are a different population having ellipsoidal shapes and a more orthodox matrix structure. Membrane potential measurements were confined to the mitochondria in the neurites because their uniform diameters and orientations made them ideal for the model-based correction procedures.

Fluorescent intracellular probes can act as sensitizers to produce singlet oxygen which, in turn, can produce a variety of toxic oxygen radicals. This mechanism also plays an important role in photobleaching, since the radicals react with probe molecules. By limiting the total dose of light exposure that a cell can withstand, these processes place limitations on the spatial and temporal information that can be obtained in fluorescence microscopy of living cells (Tsien and Waggoner, 1990). In confocal microscopy, the fluorescence excited from out of the plane of focus is rejected from the acquired image; this inherent inefficiency accentuates the difficulty of obtaining high resolution 3D or time-dependent data on living cells that cannot be treated with the toxic antioxidants that are routine components of the recipes used to fix microscopic specimens (Bacallao et al., 1990). Ultimately, such practical considerations confounded attempts to extend our earlier measurements of V_{mit} with confocal microscopy (Farkas et al., 1989; Loew, 1993). An important advantage of the widefield microscopy approach described in this paper is that *all* of the fluorescence collected by the microscope objective is detected and the computational procedure is then used to accurately restore out-of-focus light to its correct plane. This made it possible to obtain a time series of 3D images with up to 84 separate exposures to laser excitation.

Bleaching and/or phototoxicity do limit the amount of data that can be obtained from mitochondria that have been stressed with uncouplers or respiratory inhibitors. Only one or two 3D images ($\leq$14 exposures) could be obtained in the presence of 0.1 μM FCCP or 1 μM antimycin A before obvious bleaching of TMRE and mitochondrial swelling. An unexposed region of the same neurite is not affected, indicating that the damage is dependent on both light and the presence of the drug. This interesting observation suggests that the mitochondria actively scavenge oxygen radicals, probably via the known superoxide dismutase-dependent pathway (Beyer et al., 1991), and that this process is dependent on a normal level of electron transfer activity within the matrix. When the mitochondria are stressed, regulatory controls may divert all activity toward full respiration and away from ancillary functions such as free radical annihilation. This interpretation is also consistent with studies showing directly that reactive oxygen species are produced during respiration and that this activity is potentiated in the presence of uncouplers or antimycin A (Boveris and Chance, 1973; Boveris, 1976).

Another methodological difficulty that had to be overcome to extend our earlier work arose because of the high motility of mitochondria in living cells. Since the method required measurement of fluorescence intensities from the interior of a mitochondrion, it was necessary to be sure that the image plane was properly centered on that mitochondrion. This could be achieved by obtaining 3D images and only analyzing mitochondria that were totally within the imaged volume. However, the high motility of the mitochondria, which could approach 3 μm/s, made all existing schemes for 3D image microscopy unsuitable; the mitochondrial fluorescence is smeared over a significant number of pixels during the time required to move the microscope focus with a motor or readout image planes from a ccd or confocal scanner. Therefore, a custom-designed fast 3D microscope was used, which incorporates a piezoelectric objective positioner for rapid focus control and a frame transfer cooled ccd camera for rapid image acquisition. This device permitted us to obtain 3D images with 7 planes of data in 155 ms—fast enough so that none of the mitochondria move more than 3 pixels during acquisition. The motion of 95% of the mitochondria amounted to less than 0.5 pixel in a 155-ms period.

The time studies show that the V_{mit} of individual mitochondria is quite stable with the exception of occasional dramatic fluctuations. The small number of mitochondria that were caught displaying such fluctuations do not have anything obvious in common, having a range of resting V_{mit} values, a range of sizes and a range of motilities. It is possible, therefore, that many more mitochondria would be caught displaying such behavior if the observation time could be extended. There have been reports in the early literature of oscillatory behavior in mitochondrial suspensions in which the mitochondria have been made permeable to ions (reviewed by Gooch and Packer, 1974); the fluctuations observed in this paper are clearly not synchronized because, perhaps, of the absence of a concerted global stimulus. Nevertheless, the mechanistic origins of the phenomena may be similar.

The response of V_{mit} to moderate concentrations of FCCP and antimycin A shows that the mitochondria are rapidly depolarized to a new steady state level, which can be maintained over a prolonged period of time. The persistence of mitochondrial motility provides a convenient assay of the continued availability of ATP during these experiments. The

membrane potential remains steady over times as long as 30 min—even after motility has completely ceased. This suggests that under these conditions the level of respiratory activity cannot be regulated by the ATP/ADP ratio (Brand and Murphy, 1987); as discussed above, it appears that electron transfer is proceeding at a maximum rate to try to combat the stress induced by these agents and is not subject to further control. It would be of interest to systematically correlate the level of steady state depolarization with the time required to deplete ATP stores within these neurites. In addition, these results, along with the lack of a correlation between motility and V_{mit} in unstressed cells, imply that mitochondrial spatial distributions are not directly driven by the concentration of ATP or the ATP/ADP ratio. This is consistent with a recent study of mitochondrial transport in growing axons, which shows that mitochondrial accumulation near the growth cone is reversed when growth is blocked either physically or pharmacologically but is not dependent on mitochondrial capacity to produce ATP (Morris and Hollenbeck, 1993). The ability of the cytosolic energy state to control the distribution of mitochondria would be a worthwhile subject of future studies using the methods developed in this work.

Such detailed studies of the in situ response of mitochondria to cell physiological states and stimuli are easily accommodated by the general methodology introduced in this paper. The response of mitochondria to signal-transducing stimuli, for example, can be readily examined for the N1E-115 neuroblastoma cells without any significant modification or improvement of these procedures. A real limitation of the method, however, is the requirement for well defined and uniform size distributions to permit the derivation of model-based corrections to the measured fluorescence intensities. Alternatively, studies can be performed on cells containing mitochondria that are large enough to be bigger than the vertical resolution limit of the restored images. Clearly there are cells available to meet these criteria and offer convenient systems for the study of basic principles of mitochondrial regulation. Other limitations include the restricted rectangular geometry of the frame-transfer ccd imager and the long computation times required for the convergence of the restoration algorithms. But both of these latter problems are likely to be eliminated with the incorporation of better ccd and computer technologies, many of which are already available. It is anticipated, therefore, that this study will serve as a model for extension of quantitative multidimensional imaging microscopy to examinations of other key features of intramitochondrial physiology (e.g., pH and $[Ca^{2+}]$) in a variety of cells.

The financial support of the National Institute for General Medical Sciences (GM35063) and the National Science Foundation (BIR-9200027) is gratefully acknowledged.

The authors are indebted to Kevin Fogarty and Doug Bowman for providing the image analysis software and for their invaluable technical advice. Technical assistance was graciously provided by Kristine Perry and Mei-de Wei. Generous access to the SGI VGX computer was provided by John Carson and Frank Morgan. We are also grateful to Chris Pearson and the University of Connecticut Health Center Electron Microscopy Facility for the electron micrographs.

REFERENCES

Agard, D. A. 1984. Optical sectioning microscopy: cellular architecture in three dimensions. *Annu. Rev. Biophys. Bioeng.* 13:191–219.

Agard, D. A., Y. Hiraoka, P. Shaw, and J. W. Sedat. 1989. Fluorescence microscopy in three dimensions. *In* Methods in Cell Biology. Vol. 30. D. L. Taylor and Y. Wang, editors. Academic Press, San Diego. 353–377.

Bacallao, R., M. Bomsel, E. H. K. Stelzer, and J. De Mey. 1990. Guiding principles of specimen preservation for confocal fluorescence microscopy. *In* Handbook of Biological Fluorescence Microscopy. J. B. Pawley, editor. Plenum Press, New York. 197–205.

Beyer, W., J. Imlay, and I. Fridovich. 1991. Superoxide dismutases. *In* Progress in Nucleic Acid Research and Molecular Biology. Vol. 40. W. E. Cohn and K. Moldave, editors. Academic Press, San Diego. 221–253.

Boveris, A. 1976. Mitochondrial production of superoxide radical and hydrogen peroxide. *Adv. Exp. Med. Biol.* 78:67–82.

Boveris, A., and B. Chance. 1973. The mitochondrial generation of hydrogen peroxide. *Biochem. J.* 134:707–716.

Brand, M. D., and M. P. Murphy. 1987. Control of electron flux through the respiratory chain in mitochondria and cells. *Camb. Phil. Soc. Biol. Rev.* 62:141–193.

Carrington, W. A. 1990. Image restoration in 3D microscopy with limited data. *In* Proceedings on Bioimaging and Two Dimensional Spectroscopy. L. C. Smith, editor. SPIE, Los Angeles. 72–83.

Carrington, W., and K. E. Fogarty. 1987. 3-D molecular distribution in living cells by deconvolution of optical sections using light microscopy. *In* Proceedings of the 13th Annual Northeast Bioengineering Conference. K. Foster, editor. Institute of Electrical and Electronics Engineers, Los Angeles. 108–111.

Carrington, W., K. E. Fogarty, and F. S. Fay. 1990. 3D fluorescence imaging of single cells using image restoration. *In* Non-invasive Techniques in Cell Biology. K. Foster, editor. Wiley-Liss, New York. 53–72.

Chance, B., P. B. Boyer, L. Ernster, P. Mitchell, E. Racker, and E. C. Slater. 1977. Oxidative phosphorylation and photophosphorylation. *Annu. Rev. Biochem.* 46:955–1026.

Chen, L. B. 1988. Mitochondrial membrane potential in living cells. *Annu. Rev. Cell Biol.* 4:155–181.

Ehrenberg, B., V. Montana, M.-D. Wei, J. P. Wuskell, and L. M. Loew. 1988. Membrane potential can be determined in individual cells from the nernstian distribution of cationic dyes. *Biophys. J.* 53:785–794.

Farkas, D. L., M. Wei, P. Febbroriello, J. H. Carson, and L. M. Loew. 1989. Simultaneous imaging of cell and mitochondrial membrane potential. *Biophys. J.* 56:1053–1069.

Fay, F. S., W. Carrington, and K. E. Fogarty. 1989. Three-dimensional molecular distribution in single cells analyzed using the digital imaging microscope. *J. Microsc. (Oxf.).* 153:133–149.

Ferguson, S. J. 1985. Fully delocalised chemiosmotic or localised proton flow pathways in energy coupling? A scrutiny of experimental evidence. *Biochim. Biophys. Acta.* 811:47–95.

Forman, D. S., K. J. Lynch, and R. S. Smith. 1987. Organelle dynamics in lobster axons: anterograde, retrograde and stationary mitochondria. *Brain Res.* 412:96–106.

Gooch, V. D., and L. D. Packer. 1974. Oscillatory systems in mitochondria. *Biochim. Biophys. Acta.* 346:245–260.

Johnson, L. V., M. L. Walsh, B. J. Bockus, and L. B. Chen. 1981. Monitoring of relative mitochondrial membrane potential in living cells by fluorescence microscopy. *J. Cell Biol.* 88:526–535.

Kimhi, Y., C. Palfrey, I. Spector, Y. Barak, and U. Littauer. 1979. Maturation of neuroblastoma cells in the presence of dimethylsulfoxide. *Proc. Natl. Acad. Sci. USA.* 73:462–466.

Loew, L. M. 1993. Confocal microscopy of potentiometric fluorescent dyes. *In* Cell Biological Applications of Confocal Microscopy. Methods in Cell Biology. Vol. 38. B. Matsumoto, editor. Academic Press, Orlando. 195–209.

Martz, D., R. J. Lasek, S. T. Brady, and R. D. Allen. 1984. Mitochondrial motility in axons: membranous organelles may interact with the force generating system through multiple binding sites. *Cell Motil.* 4:89–101.

Mitchell, P. 1961. Coupling of phosphorylation to electron and hydrogen

transfer by a chemi-osmotic type of mechanism. *Nature (Lond.)*. 191: 144–148.

Morris, R. L., and P. J. Hollenbeck. 1993. The regulation of bidirectional mitochondrial transport is coordinated with axonal growth. *J. Cell Sci.* 104:917–927.

Nicholls, D. G. 1982. Bioenergetics. An Introduction to the Chemiosmotic Theory. Academic Press, London.

Reers, M., T. W. Smith, and L. B. Chen. 1991. J-aggregate formation of a carbocyanine as a quantitative fluorescent indicator of membrane potential. *Biochemistry*. 30:4480–4486.

Scalettar, B. A., J. R. Abney, and C. R. Hackenbrock. 1991. Dynamics, structure, and function are coupled in the mitochondrial matrix. *Proc. Natl. Acad. Sci. USA*. 88:8057–8061.

Singer, T. P. 1979. Mitochondrial electron-transport inhibitors. *Methods Enzymol.* 55:454–462.

Smiley, S. T., M. Reers, C. Mottola-Hartshorn, M. Lin, A. Chen, T. W. Smith, G. D. Steele, and L. B. Chen. 1991. Intracellular heterogeneity in mitochondrial membrane potentials revealed by a J-aggregate-forming lipophilic cation JC-1. *Proc. Natl. Acad. Sci. USA*. 88: 3671–3675.

Smith, J. C. 1988. Potential-sensitive molecular probes in energy-transducing organelles. *In* Spectroscopic Membrane Probes. Vol. 2. L. M. Loew, editor. CRC Press, Boca Raton, FL. 153–191.

Tedeschi, H. 1980. The mitochondrial membrane potential. *Camb. Phil. Soc. Biol. Rev.* 55:171–206.

Tsien, R. Y., and A. Waggoner. 1990. Fluorophores for confocal microscopy: photophysics and photochemistry. *In* Handbook of Biological Confocal Microscopy. J. B. Pawley, editor. Plenum Press, New York. 169–178.